Lab on a Chip

Accepted Manuscript

This article can be cited before page numbers have been issued, to do this please use: W. Lee, Y. Park, J. Park, S. Shrivastava, Y. M. Son, H. Choi, J. Lee, B. Jeon, L. Heon and N. E. Lee, *Lab Chip*, 2019, DOI: 10.1039/C8LC01344F.

This is an Accepted Manuscript, which has been through the Royal Society of Chemistry peer review process and has been accepted for publication.

Accepted Manuscripts are published online shortly after acceptance, before technical editing, formatting and proof reading. Using this free service, authors can make their results available to the community, in citable form, before we publish the edited article. We will replace this Accepted Manuscript with the edited and formatted Advance Article as soon as it is available.

You can find more information about Accepted Manuscripts in the author guidelines.

Please note that technical editing may introduce minor changes to the text and/or graphics, which may alter content. The journal's standard Terms & Conditions and the ethical guidelines, outlined in our author and reviewer resource centre, still apply. In no event shall the Royal Society of Chemistry be held responsible for any errors or omissions in this Accepted Manuscript or any consequences arising from the use of any information it contains.

ROYAL SOCIETY OF CHEMISTRY

rsc.li/loc

ROYAL SOCIETY OF CHEMISTRY View Article Online
DOI: 10.1039/C8LC01344F

Lab on a Chip

PAPER

Smartphone fluorescent imaging-based mobile biosensing system integrated with passive fluidic control cartridge for minimal user intervention and high accuracy

Received 00th January 20xx,
Accepted 00th January 20xx

DOI: 10.1039/x0xx00000x

rsc.li/loc

Won-Il Lee[a], Younghyeon Park[d], Jaemin Park[e], Sajal Shrivastava[b], Young-Min Son[a], Hak-Jong Choi[f], Jaelin Lee[d], Byeungwoo Jeon[d], Heon Lee*[e] and Nae-Eung Lee*[abc]

A key challenge for realizing mobile device-based on-the-spot environmental biodetection is that a biosensor integrated with fluid handling sensor cartridge must have acceptable accuracy comparable to that of conventional standard analytical methods. Furthermore, the user interface must be easy to operate, technologically plausible, and concise. Herein, we introduce an advanced smartphone imaging-based fluorescent microscope designed for Hg^{2+} monitoring by utilizing a biosensor cartridge that reduces user intervention via a time-sequenced passive fluid handling. The cartridge also employs a metal-nanostructured plastic substrate for complementing the fluorescent signal output, helping to realize a high-accuracy detection in which a ratiometric dual-wavelength detection method is applied. Using 30 samples of Hg^{2+}-spiked wastewater, we have shown that our device, which has a detection limit of ~1 pM, can perform analytical assays accurately. The detection results from our method were in good linearity and agreement with those of conventional standard methods. We conclude that the integration of a simple-to-use biosensor cartridge, fluorescence signal enhancing substrate, dual-wavelength detection, and quantitative image data processing on a smartphone has great potential to make any population accessible to small molecule detection, which has been performed in centralized laboratories for environmental monitoring.

Introduction

With the continuing progress in the state-of-the-art technology of smartphones, a number of researchers have utilized the high-quality camera, mobile computing, connectivity and compactness of the device to build biosensors having optical, easily accessible spatiotemporal data, and portable features[1-9] for fulfilling diagnostic point-of-care testing (POCT) or on-the-spot environmental detection. A key challenge on POCT or on-the-spot environmental detection is that a biosensor integrated with a smartphone must have high sensitivity and specificity and a detection accuracy that is comparable to that of conventional standard analytical methods. Moreover, its user interface, when used on the spot, must be easy to operate, technologically plausible, and concise.

In view of the abovementioned requirements, many biosensing platforms including microfluidic paper-based analytical devices or lateral flow assays considering passive fluid manipulations such as fluid velocity control[10-12] and controlled fluid flow with valve[13-15] or hand actuation[16, 17] have been mainly investigated for user convenience and minimal intervention. However, information on their diagnostic performance compared to standard methods is still lacking. On the other hand, there have been some reports on user-convenient devices based on lab-on-a-chip platforms with field-acceptable sensitivity, specificity, and detection accuracy for infectious sexually transmitted diseases[18] and human semen[19] diagnosis, respectively. However, with respect to detection mechanisms applied to both works (colorimetric immunoassay and cell counting), it is difficult to handle the detection of heavy

[a]Samsung Advanced Institute for Health Sciences & Technology (SAIHST), Sungkyunkwan University, Suwon, Gyeonggi-do 16419, Republic of Korea
[b]School of Advanced Materials Science & Engineering, Sungkyunkwan University, Suwon, Gyeonggi-do 16419, Republic of Korea
[c]SKKU Advanced Institute of Nanotechnology (SAINT), Sungkyunkwan University, Suwon, Gyeonggi-do 16419, Republic of Korea
E-mail: nelee@skku.edu
[d]Department of Electrical and Computer Engineering, Sungkyunkwan University, Suwon, Gyeonggi-do 16419, Republic of Korea
[e]Department of Material science and Engineering, Korea University, Seoul 02841, Republic of Korea
E-mail: nanoimprint@naver.com
[f]Electrical & Systems Engineering, University of Pennsylvania, Philadelphia, PA 19104, USA
†Electronic supplementary information (ESI) available: Methods, supplementary movies, figures, and tables. See DOI: 10.1039/x0xx00000x

View Article Online
DOI: 10.1039/C8LC01344F

metal ions as contaminants in water in addition to small molecules, which require alternative schemes for biosensors to obtain a high detection accuracy by satisfying environmental diagnosis at low cut-off values in the field.

Recently, smartphone fluorescent microscopy has been a preferred signal readout tool because of its advantages such as nano-to-micro-scaled resolution, low limit of detection (LOD), and multiplexing capability on visible bands[4, 20-23]. Additionally, detection accuracy can be enhanced by utilizing a dual-wavelength "seesawed" fluorescence detection scheme using aptamer probes[24, 25]. Even though fluorescent detection strategies are suitable for highly sensitive and accurate detection, the question of whether the technology in the laboratory can be translated into the real world remains unsolved due to multiple user interventions from target sample loading to resulting data output[26]. In detail, laboratory-based technologies mostly include serial pipetting for removing and washing target molecules and unbound reagents to suppress background noise in the interest of high signal-to-noise ratio (SNR), which is overly dependent upon an individual's skill and considerably far from an ideal POCT or on-the-spot detection devices.

In order to overcome such challenges, we introduce a new biosensor cartridge platform for the control of biochemical detection with passive regulation of reaction incubation time. This biosensor cartridge provides tunability in controlling the incubation time of target-probe reactions by modifying the dimension of the key part as well as the immediate, sequential, and passive sample removal and washing as a way of minimizing user intervention. Hence, integrating this cartridge with a smartphone fluorescent microscope (SFM), which utilizes an imaging-based dual-wavelength "seesawed" ratiometric detection for improvement of detection accuracy by minimizing false signals (similar to the concept introduced in our previous work[24], can provide notable improvements in user interface and detection accuracy comparable to those of conventional methods. The significance of this work is present at Table 1.

Here, we focus on the advancement of smartphone fluorescent microscopy in terms of easy operation and field-acceptable performance by demonstrating the dual-wavelength fluorescence quantitative detection of mercury ion (Hg^{2+}) with thymine (T)-mismatched deoxyribonucleic acid (DNA) probes[6, 27, 28] on an integrated biosensor cartridge. We developed the biosensor cartridge composed of low-cost materials such as water-soluble double-sided tape, cotton linter absorption pad, and polyolefin film. Because the cartridge was designed to be adherable to arbitrary substrates, we utilized a nanometalized plastic substrate to obtain a larger dynamic range and LOD resulting from an enhanced SNR due to an increase in fluorescence intensity by a combination of metal-enhanced fluorescence (MEF) and surface plasmon. For the quantitative processing of fluorescence image data, a custom-built smartphone add-on type epifluorescence microscope was prototyped as a fluorescent image reader and an android smartphone app, which allows fluorescent images taken from the sample-reacted biosensor cartridge to be processed and reports detection results set upon a pre-embedded calibration curve, was created. In accordance with the confirmation of low LOD (1 pM) below the maximum contaminant level of mercury ion regulated for drinking water (~10 nM, 2 ppb by US EPA[29], 6 ppb by the World Health Organization[30]) from our device, we conducted analytical assay tests with spiked samples using wastewater and compared the accuracy of the test to the results obtained from a field standard method of atomic absorption spectrometry. Detection results from our method and those of laboratory-based conventional method were in good agreement, with the area under the receiver operating characteristic (ROC) curve (AUC) of our device (0.983) comparable to that of the conventional method (1.0).

Table 1 Significance of this work in comparison with the recently published reports of smartphone-based heavy metal sensors in aspect of user-convenience and accuracy

Detection target	Test method	User-convenience	Quantitative accuracy with low cut-off value	Ref.
Ni(Ⅱ), Cu(Ⅱ), Cd(Ⅱ) and Cr(Ⅳ)	Colorimetric	Medium	N.A.	31
Hg(Ⅱ)	Colorimetric	Medium	N.A.	6
Cr(Ⅲ)	Colorimetric	Low	N.A.	32
Hg(Ⅱ)	Fluorescence/ Colorimetric	High	N.A.	33
Hg(Ⅱ)	Fluorescence	High	AUC : 0.983	This work

Experimental section

Reagents and chemicals

Hg^{2+} DNA probe (P1, 5′-Amino modifier-C12-CTTCTTTCTT-3′), Hg^{2+} DNA pair probe (P2, 5′-Biotin-TTGTTTGTTG-3′), and complementary DNA (5′-AAGAAAGAAG-3′) were purchased (Integrated DNA Technologies). P1 and complementary sequence were mixed in equimolar concentration of 100 μM and annealed to hybridize in 1× phosphate-buffered saline (PBS) buffer. P2 was incubated with Qdot 655 streptavidin conjugate (ThermoFisher) with a concentration ratio of 5:1 for 1 h in 50 mM borate buffer with 1% bovine serum albumin purchased from Sigma Aldrich, and the conjugates were purified with a spin-column chromatography (MICROSPIN G-50 COLUMNS, GE Healthcare). Standard mercury (1000 mg/L), $PbCl_2$, $ZnCl_2$, $CuCl_2$, $MgCl_2$, $FeCl_3$, $PdCl_2$, and $HAuCl_4$ were purchased from Sigma-Aldrich.

Paper Lab on a Chip
View Article Online
DOI: 10.1039/C8LC01344F

Fabrication of nano-metalized array on plastic substrate and biosensor cartridge

A Si master stamp containing a square array of nanohole pattern with various pitches and diameters was prepared using a conventional photolithography and reactive ion etching process. Prior to hot embossing process, the surface of the Si master stamp was coated with a self-assembled monolayer using heptadecafluoro-1,1,2,2-tetra-hydrodecyltrichlorosilane (HDFS) to reduce the surface energy of the Si master stamp and facilitate the subsequent detachment of the Si master stamp. To fluorinate the surface of the Si master stamp using HDFS solution, the Si master stamp was cleaned by ethanol and acetone and was exposed UV-O_3 treatment for 10 min. Then, the Si master stamp was dipped into an HDFS-based solution diluted with hexane at 1:1000 volume ratio. Next, the Si master stamp was rinsed with hexane and deionized water alternately and was dried with N_2 gas. Then, a square array of nanopillars was fabricated on a polycarbonate substrate using a hot embossing process. The Si master stamp was contacted on the cleaned bare polycarbonate substrate and loaded into the hot embossing system. The embossing system is composed of a heating plate and a pressurizing chamber. The hot embossing process was performed under pressure in low vacuum. The Si master stamp is put into conformal contact with the bare polycarbonate substrate and then heated between the glass transition temperature (T_g) and melting temperature of approximately 130 °C for 20 min to increase the viscosity of the polycarbonate substrate. Subsequently, a pressure of 10 bar was applied uniformly between them to transform the polycarbonate substrate. The polycarbonate substrate that was heated above the T_g and was viscous can be used to fill the square nanohole array pattern of the Si master stamp using an applied pressure and capillary force. After the polycarbonate substrate was transformed to match the surface of the Si master stamp, the embossing system was cooled to room temperature. Finally, the Si master stamp was physically detached from the polycarbonate substrate with a nanopillar array. As a result, the square nanopillar array was successfully fabricated onto the polycarbonate substrate with high fidelity, and the size of the patterned area was 1 × 1 cm^2. Then, a 100 nm thick silver thin film with 5 nm thick Cr as an adhesion layer was deposited by using an e-beam evaporation system followed by deposition of 30 nm thick Al_2O_3 layer as a spacer in the atomic layer deposition system.

The following materials were used for the cartridge: CF7 absorption pad (Whatman), water-soluble double-sided tape (SUNfabric, South Korea), water-insoluble organic film composed of polyolefins and paraffin waxes (Bemis Company). The precise cutting for apertures of the cartridge was carried out with a laser cutter (Universal Laser Systems). The cartridge was adhesively bonded on the fabricated nanometalized polycarbonate substrate, where fluorescent dye intercalated P2-cDNA duplex is immobilized in the center via amination with 3% (3-aminopropyl) triethoxysilane (Alfa Aesar) in ethanol for 30 min, formation of aldehyde groups with 2.5% glutaraldehyde (Polyscience) in pH 7.4 PBS buffer for 30 min, and microspotting using a 0.2 mm diameter pin (Xact II microarrayer, Labnext).

Hardware and software of SFM

The housing of SFM including the microscope body and inserting stage was manufactured using a 3D printer (CUBICON Style, CUBICON, South Korea). Objective lens of 10×, RMS thread adapter for objectives, and 12× eyepiece were purchased from Edmund Optics. Bandpass filters of 650/13 nm, 520/5 nm, and 447/60 nm were purchased from Semrock. Dovetail translation stage, USAF1951 wheel pattern positive, dichroic mirror with 490 nm cutoff, silver mirror, 462 nm multi-mode laser diode with its collimation package and electrostatic discharge protection, microscope stage micrometer, and circle tophat diffuser were purchased from Thorlabs. The laser beam was powered by a portable power bank with USB 5 V output and capacity of 5000 mAh (Mi power bank, Xiaomi). The application software was developed to provide functionalities of image capture, processing, and result display. The image capture part was implemented by a camera application programming interface in the android software development kit to control the setting values of the camera device. The captured images were the raw sensor data, which are obtained by the image signal processor (ISP) operation in the smartphone. In the camera setting, the auto exposure was turned off to obtain the linearly increasing and decreasing value of image from the changing of fluorescence intensity of sample. The shutter speed and ISO values were fixed as 1/45 s and 250, respectively, to avoid under and over saturation of the image. After obtaining raw data, the image was cropped from 5238 × 3000 pixels to 2048 × 2048 pixels to minimize the space/computational complexity in the process of image processing. The proposed image processing, such as demosaicking, grayscale conversion, region of interest (ROI) search, and measurement were implemented on the smartphone (see ESI†) and it was designed so that the result is finally displayed on the screen. The process of searching and registering the intensity value in the ROI was empirically determined from the captured fluorescent image of samples with different Hg^{2+} concentrations.

Analytical assay with Hg^{2+} spiked wastewater samples

We collected the wastewater sample from the water treatment plant of Sungkyunkan University. For spiking different concentrations of Hg^{2+}, 10 aliquots were made and the measurement was repeated three times with SFM and cold vapor atomic absorption spectrometry (CVAAS) for the same spiked samples. For the assay of SFM, 100 µL spiked sample was taken to the biosensor cartridge and readout data were obtained and decided when the result is displayed to “take” in app operation. Meanwhile, the same samples measured by SFM were taken for quantifying detection with CVAAS instrument (Tekran Model 2600, Tekran, Canada) on the same day. MedCalc statistical software was used to carry out Passing–Bablok[34], Bland–Altman[35], and ROC curve analysis with measured data from two different methods.

View Article Online
DOI: 10.1039/C8LC01344F

Results and discussion

Smartphone imaging-based user-convenient fluorescent sensing platform

We developed an optical biosensing platform in the shape of a reader with a chip insertion slit consisting of an SFM and an insertable biosensor cartridge, as depicted in Fig. 1. To demonstrate this platform with Hg^{2+}, we employed T–T-mismatched DNA probes as capture molecule for Hg^{2+}. Hg^{2+} DNA probe (P1) hybridized with complementary DNA and fluorescent-dye intercalated is immobilized on a nanometalized substrate at the center of the biosensor cartridge in the form of a microspot. When the Hg^{2+} target sample with reagent solution, which is composed of Hg^{2+} DNA probe pair (P2) conjugated quantum dot (QD), is placed in the center pod of the cartridge, the incubation for target reaction begins (Fig. 1a). After sample purging driven by capillary force without user intervention followed by completion of incubation, P1 complex is dehybridized by releasing complementary DNA and intercalating fluorescent dye; then, it forms a new complex with P2-conjugated QD according to Hg^{2+} bridging between Ts from P1 and P2 (Fig. 1b). The residual reagent is washed with drips of washing buffer, which flow toward the outer circumference in the pod where absorption is performed passively, and finally yielding a dual-wavelength fluorescent detection introduced as an enhancement tool for detection accuracy[24, 25] (Fig. 1c).

Eventually, the cartridge, which completed the reaction and washing steps, is inserted into a slit on the stage of Samsung Galaxy S6 mountable fluorescent microscope for fluorescent image acquisition at two channels of green (520 nm) and red (655 nm), and these images are analyzed in an android app algorithm for quantification and user readout (Fig. 1d).

As the cartridge provides the simplicity in design to user which can reduce the user interventions in various biosensing strategies and facilitate user-convenient operation while securing the detection accuracy, this work is distinguished from our previous works[24, 25] based on manual procedures requiring skilful techniques. Improvement of user-convenience with comparable detection accuracy to the standard method which can enable non-experts to use easily is the key challenge for smartphone-based POCT devices to be spread in the field.

Metal-enhanced fluorescence on nanometalized plastic substrate

In order to utilize the smartphone camera as an accurate fluorescent biosensor reader, it is important to obtain abundant and consistent transduction signals in accordance with the target concentration reacted on the biosensor. Enhancement of fluorescent signal is a good option to meet the conditions and solve the problem that a smartphone camera has a low SNR in low-lighting setup similar to fluorescent imaging because of its small-sized image sensor. Because we have chosen fluorophores of Sybr Green I (SGI) and QD, which have two orders of magnitude difference in their extinction coefficients, i.e., E_{495} = 75,000 $M^{-1}\cdot cm^{-1}$ [36] and E_{488} = 2,900,000 $M^{-1}\cdot cm^{-1}$, respectively, it was required to make up the fluorescent intensity level from the image at the green channel to obtain a dynamic range as broad as that from the image at the red channel, which has a highly bright emission from QD, by enhancing the emission of SGI-intercalated DNA probe. As shown in Fig. S1†, the nanometalized substrates made by the hot embossing technique and thin film deposition were optimized for maximum MEF by varying the diameter (D) and period (P) of nanopillar pattern on the polycarbonate substrate. Geometric data of the substrate with a pattern of D = 300 nm, P = 500 nm, and approximately 87 nm of height were observed by field-emission scanning electron microscopy (FESEM) (Fig. 2a) and atomic force microscopy (AFM) (Fig. 2b) for two-dimensional and three-dimensional views, respectively. The substrate with this pattern had the highest fluorescent enhancement of SGI-intercalated DNA probe among different patterns, exceeding by a factor of approximately 9 compared to the intensity of the control substrate that has only a metal thin film without nanopattern (Fig. 2c) but still shows a huge enhancement (14.5 times) by itself compared to that of a normal glass substrate [24]. The difference in enhancement can be determined not only by the number of fluorophores and surface plasmon resonance per unit area (D = 300 nm vs. D = 400 nm) but also by the high efficiency of MEF with surface plasmon coupling. The overlap of excitation band of SGI (λ_{ex} = 497) with the absorbance spectra of each substrate (Fig. 2d) predicts a similar trend with respect to SP coupling and fluorescence enhancement [37, 38]. On the condition that the nanopattern array with different geometric variations can affect the shift of SP coupling band, a near-field enhancement of light source (blue bar shown in the inset of Fig. 2d) can increase the excitation of SGI molecules and the emission is enhanced due to the increase in the quantum yield of radiative and non-radiative transitions according to the significant role of surface plasmon coupling in MEF [39].

Novel biosensor cartridge with passive regulation of reaction incubation time

We created a biosensor cartridge that can be fabricated simply and operated with concise procedure without complicated intervention by user while producing stable results by combining the advantages of the paper-based device, which has passive regulation, to those of lab-on-a-chip device, which has volume controllability. The cartridge is made of low-cost materials such as water-soluble double-sided tape, absorbent pad, and water-insoluble organic film layer as shown in Fig. 3a. For operation, 100 µL of target sample mixture is dropped in the center pod of the cartridge and it starts to disintegrate into a time barrier, which is a water-soluble double-sided tape (Fig. 3b), until the disintegration by the sample solution reaches the absorbent pad across the junction of the water-insoluble layer and water-soluble tape. Once the sample solution comes in contact with the absorbent pad, immediately, it is purged by a passively driven capillary force of the pad as shown in Fig. 3c. The actual operation of the cartridge over time is presented as a time-series pictures in Fig. 3d and a video in Movie S1†. After purging, a simple washing step is also

View Article Online
DOI: 10.1039/C8LC01344E

provided as shown in Movie S2†. Notably, the cartridge can be placed on an arbitrary substrate after peeling off the protection film of the tape and the time for sample confinement in the center pod can be controlled. This is because the water-soluble double-sided tape, as the key material in our design, is attached to the bottom of the center-holed absorbent pad, which is sandwiched by the upper water-insoluble layer and cut in the center leaving annulus of the junction of two layers from the pad. When the cartridge is integrated with the probe-spotted substrate, the confinement time of the sample becomes the incubation time for the target-probe reaction. Fig. 3e shows that the incubation time of the cartridge can be controlled by manipulating the annulus area of the junction from the pad. It is important for the realization of a simple POC tool that this cartridge does only require one-way simple operations such as loading the sample and washing the surface.

Hg^{2+} quantification on SFM integrated with biosensor cartridge

SFM was designed by considering an optical configuration allowing it to work as an epifluorescence microscope, which is the most common and powerful analytical tool for monitoring molecular reaction by using various fluorophores[40, 41]. Based on its straightforward concept, SFM was prototyped by using a 3D printer inexpensively, portably, and robustly (Fig. S2a†). As depicted in Fig. S2b†, the form factor was determined to maximize portability while the objective lens and the eyepiece were matched within the light path to obtain a high resolution (~2 μm) and wide field of view (~1.5 mm in diameter) (Fig. S3a and S3b†). For the fluorescent mode, when the mounted laser at the side of the body illuminates and excites fluorophores on the cartridge substrate inserted in the stage via dichroic mirror reflection, the generated fluorescence emission passes through the dichroic mirror, eyepiece, and emission filter and is then finally transmitted to the image sensor of the smartphone camera. This setting helped to precisely quantify the change of fluorescent intensity from restricted sensing area within a field of view by obtaining crisp and well-defined fluorescent image with low background noise due to high resolution and monochromatic excitation of laser. Fluorescent imaging was performed at two channels, as shown in Fig. 4a. During the reaction of the biosensor cartridge with 100 nM Hg^{2+} solution, the fluorescent intensity at the probe-printed microspot in the green channel decreases according to the SGI release from dehybridized P1 compared to the control. On the contrary, the intensity in the red channel increases by forming the complex of P1–Hg^{2+}–P2-conjugated QD. After acquiring fluorescent images in both channels with various target concentrations from 0 to 10 μM(Fig. S4†), we could plot standard curves at each wavelength by means of relative fluorescence ($\Delta F/F_0$) vs. concentration, which shows a wide dynamic range (from 1 pM to 1 μM) powered by the nanostructured MEF substrate as shown in Fig. 4b. A three-parameter logistic regression was applied for the nonlinear curve fitting resulting in $y = 2.47 + 1.61 \ln(x + 0.48)$ ($R^2 = 0.9965$) and $y = 0.854 - 0.047\ln(x + 0.015)$ ($R^2 = 0.9909$) at the red and green channels, respectively. LOD was determined as 1.14 pM at the red channel and 0.323 pM at the green channel by using the previously introduced method[42, 43], where the LOD of a sensor is calculated as $3.3 \times \sigma_{\text{baseline}} / slope$. Notably, the LOD values from both curves are significantly lower than the maximum contaminant level of Hg^{2+} (~10 nM, 2 ppb) established by EPA, so that we could conduct an analytical assay test. Along with the verification of sensitivity, selectivity was also confirmed with the tests that add diverse metal ions such as lead, zinc, copper, magnesium, iron, palladium, and gold evenly with the mixture, as illustrated in Fig. S5†.

We created an Android app that can take a fluorescent image at the green and red channels, process those images to obtain specific signals from the ROI, which is a fluorescing probe-printed microspot (circle dash line in Fig. 4a), and match up the processed signals of both channels to each curve registered as an algorithm into the app (Fig. 4b), which uses a simplified ISP operation such as demosaicking, grayscale conversion, ROI search, and measurement. Finally, it displays a detection result that contains the information of concentration readouts from each channel and coefficient of variation from the two readouts to decide whether to "take" or "discard" the detection result, where 5% of the coefficient of variation limit was set for the threshold of judgment (Fig. 4c).

Analytical assay test of SFM in comparison to conventional method with Hg^{2+} spiked wastewater sample

We carried out an analytical assay of 10 different concentrations of Hg^{2+}-spiked wastewater samples (n = 3, total 30 samples), which were collected from the wastewater treatment plant in our university, to evaluate whether the analytical performance of SFM can be on par with conventional standard method, i.e., CVAAS. Table S1† presents the statistical analytical assay data from both methods verifying the recovery rate and relative standard deviation (RSD) of three measurements at each concentration. We confirmed that CVAAS as a standard method flawlessly performed 100% recovery rate in 7 out of 9 samples and RSD below 7%; meanwhile, our SFM showed a recovery rate ranging from 87% to 121% and RSD below 15%. However, a close agreement between the two methods was observed with the next two analyses. In the Passing–Bablok analysis illustrated in Fig. 5a, the results showed an intercept A value of −0.0977 as systematic differences with a 95% confidence interval of −0.6577 to 0.3471 and a slope B value of 1.064 as proportional differences with a 95% confidence interval of 0.9602 to 1.1873. The cumulative sums test for linearity[44] indicated no significant deviation from linearity with P = 0.53. The Bland–Altman analysis in the format of plot differences as percentage shown in Fig. 5b showed a mean difference of 3.5% and the measurements lie within the limit of agreement, which is defined as the mean difference plus or minus 1.96 times the standard deviation of the differences when comparing SFM to CVAAS. We evaluated the detection accuracy of our SFM with the Hg^{2+} concentration threshold of 10 nM, comparing against CVAAS. The sensitivity and specificity of SFM from the assays were 80% and 91.7%, respectively. On the other hand, CVAAS showed a 93.3% of sensitivity and 100% of specificity as shown in Fig. 5a and 5b, respectively. The observed AUC was 1.0 for CVAAS and 0.983 for

SFM (Fig. 5c), which indicates that our SFM was able to accurately detect Hg^{2+} spikes in wastewater samples based on maximum contaminant level of EPA guideline. These results suggest high comparability of SFM to CVAAS.

View Article Online DOI: 10.1039/C8LC01344F

Conclusions

In this work, we introduced an SFM for Hg^{2+} sensing with notable advancement in terms of easy operation and field-acceptable performance as a POCT tool. For easy operation of the sensing implement, we built a novel biosensor cartridge, which provides not only tunability in controlling the incubation time for target-probe reaction but also an immediate, sequential and passive sample removal and washing. This was integrated onto a metal-nanostructured substrate, which can greatly enhance the fluorescent signal of green fluorophore by approximately 9 times compared to the planar substrate for making up the dynamic range at the green channel as broad as the red channel and reach an LOD of as low as 1 pM at both channels. An android app-driven SFM imaging-based dual-wavelength ratiometric detection was utilized to improve the detection accuracy so that the analytical assay can be conducted. From the statistical analysis, the detection results of SFM have an excellent linearity and were in close agreement with those of CVAAS. Moreover, the results showed a high accuracy (AUC = 0.983), which is comparable to that of CVAAS (AUC = 1.0). By achieving easy operation and high accuracy for small molecule detection, our approach may be a breakthrough to address unmet demands for the commercialization of mobile fluorescent biosensors.

Conflicts of interest

There are no conflicts to declare.

Acknowledgements

This research was supported by the Nano Material Technology Development Program (NRF-2016M3A7B4910554) and Global Ph.D Fellowship Program (NRF-2015H1A2A1034159) through the National Research Foundation of Korea (NRF)

References

1. K. Yamada, D. Citterio and C. S. Henry, *Lab on a Chip*, 2018, **18**, 1485-1493.
2. A. Soni, R. K. Surana and S. K. Jha, *Sensors and Actuators B: Chemical*, 2018, **269**, 346-353.
3. J.-S. Yang, J. Shin, S. Choi and H.-I. Jung, *Sensors and Actuators B: Chemical*, 2017, **241**, 80-84.
4. K. Ming, J. Kim, M. J. Biondi, A. Syed, K. Chen, A. Lam, M. Ostrowski, A. Rebbapragada, J. J. Feld and W. C. W. Chan, *ACS Nano*, 2015, **9**, 3060-3074.
5. M. V. D'Ambrosio, M. Bakalar, S. Bennuru, C. Reber, A. Skandarajah, L. Nilsson, N. Switz, J. Kamgno, S. Pion, M. Boussinesq, T. B. Nutman and D. A. Fletcher, *Science Translational Medicine*, 2015, **7**, 286re284.
6. Q. Wei, R. Nagi, K. Sadeghi, S. Feng, E. Yan, S. J. Ki, R. Caire, D. Tseng and A. Ozcan, *ACS Nano*, 2014, **8**, 1121-1129.
7. S. Choi, S. Kim, J.-S. Yang, J.-H. Lee, C. Joo and H.-I. Jung, *Sensing and Bio-Sensing Research*, 2014, **2**, 8-11.
8. Y. Sekine, S. B. Kim, Y. Zhang, A. J. Bandodkar, S. Xu, J. Choi, M. Irie, T. R. Ray, P. Kohli, N. Kozai, T. Sugita, Y. Wu, K. Lee, K.-T. Lee, R. Ghaffari and J. A. Rogers, *Lab on a Chip*, 2018, **18**, 2178-2186.
9. J. Song, V. Pandian, M. G. Mauk, H. H. Bau, S. Cherry, L. C. Tisi and C. Liu, *Analytical Chemistry*, 2018, **90**, 4823-4831.
10. B. Lutz, T. Liang, E. Fu, S. Ramachandran, P. Kauffman and P. Yager, *Lab on a Chip*, 2013, **13**, 2840-2847.
11. C. Renault, X. Li, S. E. Fosdick and R. M. Crooks, *Analytical Chemistry*, 2013, **85**, 7976-7979.
12. C. Renault, J. Koehne, A. J. Ricco and R. M. Crooks, *Langmuir*, 2014, **30**, 7030-7036.
13. B. J. Toley, J. A. Wang, M. Gupta, J. R. Buser, L. K. Lafleur, B. R. Lutz, E. Fu and P. Yager, *Lab on a Chip*, 2015, **15**, 1432-1444.
14. R. Gerbers, W. Foellscher, H. Chen, C. Anagnostopoulos and M. Faghri, *Lab on a Chip*, 2014, **14**, 4042-4049.
15. S. Jahanshahi-Anbuhi, A. Henry, V. Leung, C. Sicard, K. Pennings, R. Pelton, J. D. Brennan and C. D. M. Filipe, *Lab on a Chip*, 2014, **14**, 229-236.
16. R. Robinson, L. Wong, R. Monnat and E. Fu, *Micromachines*, 2016, **7**, 28.
17. C. G. Li, H.-A. Joung, H. Noh, M.-B. Song, M.-G. Kim and H. Jung, *Lab on a Chip*, 2015, **15**, 3286-3292.
18. T. Laksanasopin, T. W. Guo, S. Nayak, A. A. Sridhara, S. Xie, O. O. Olowookere, P. Cadinu, F. Meng, N. H. Chee, J. Kim, C. D. Chin, E. Munyazesa, P. Mugwaneza, A. J. Rai, V. Mugisha, A. R. Castro, D. Steinmiller, V. Linder, J. E. Justman, S. Nsanzimana and S. K. Sia, *Science Translational Medicine*, 2015, **7**, 273re271.
19. M. K. Kanakasabapathy, M. Sadasivam, A. Singh, C. Preston, P. Thirumalaraju, M. Venkataraman, C. L. Bormann, M. S. Draz, J. C. Petrozza and H. Shafiee, *Science Translational Medicine*, 2017, **9**, eaai7863.
20. Q. Wei, H. Qi, W. Luo, D. Tseng, S. J. Ki, Z. Wan, Z. Göröcs, L. A. Bentolila, T.-T. Wu, R. Sun and A. Ozcan, *ACS Nano*, 2013, **7**, 9147-9155.
21. S. Shrivastava, W.-I. Lee and N.-E. Lee, *Biosensors and Bioelectronics*, 2018, **109**, 90-97.

22. H. C. Koydemir, Z. Gorocs, D. Tseng, B. Cortazar, S. Feng, R. Y. L. Chan, J. Burbano, E. McLeod and A. Ozcan, *Lab on a Chip*, 2015, **15**, 1284-1293.
23. S.-C. Liao, J. Peng, M. G. Mauk, S. Awasthi, J. Song, H. Friedman, H. H. Bau and C. Liu, *Sensors and Actuators B: Chemical*, 2016, **229**, 232-238.
24. W.-I. Lee, S. Shrivastava, L.-T. Duy, B. Yeong Kim, Y.-M. Son and N.-E. Lee, *Biosensors and Bioelectronics*, 2017, **94**, 643-650.
25. S. Shrivastava, N. M. Triet, Y.-M. Son, W.-I. Lee and N.-E. Lee, *Biosensors and Bioelectronics*, 2017, **90**, 450-458.
26. H. Wang, Y. Sun, W. Yue, Q. Kang, H. Li and D. Shen, *Analyst*, 2018, **143**, 1670-1678.
27. J.-S. Lee and C. A. Mirkin, *Analytical Chemistry*, 2008, **80**, 6805-6808.
28. X. Xue, F. Wang and X. Liu, *Journal of the American Chemical Society*, 2008, **130**, 3244-3245.
29. U.S.EPA, National Primary Drinking Water Regulations, https://www.epa.gov/ground-water-and-drinking-water/national-primary-drinking-water-regulations#Inorganic).
30. WorldHealthOrganization, Guidelines for Drinking-water Quality, Fourth Edition, http://www.who.int/water_sanitation_health/publications/drinking-water-quality-guidelines-4-including-1st-addendum/en/).
31. H. Wang, Y.-j. Li, J.-f. Wei, J.-r. Xu, Y.-h. Wang and G.-x. Zheng, *Analytical and Bioanalytical Chemistry*, 2014, **406**, 2799-2807.
32. S. Yu, W. Xiao, Q. Fu, Z. Wu, C. Yao, H. Shen and Y. Tang, *Analytical Methods*, 2016, **8**, 6877-6882.
33. L. Wang, B. Li, F. Xu, X. Shi, D. Feng, D. Wei, Y. Li, Y. Feng, Y. Wang, D. Jia and Y. Zhou, *Biosensors and Bioelectronics*, 2016, **79**, 1-8.
34. H. Passing and W. Bablok, *Journal*, 1983, **21**, 709.
35. J. Martin Bland and D. Altman, *The Lancet*, 1986, **327**, 307-310.
36. A. I. Dragan, R. Pavlovic, J. B. McGivney, J. R. Casas-Finet, E. S. Bishop, R. J. Strouse, M. A. Schenerman and C. D. Geddes, *Journal of Fluorescence*, 2012, **22**, 1189-1199.
37. P. P. Pompa, L. Martiradonna, A. D. Torre, F. D. Sala, L. Manna, M. De Vittorio, F. Calabi, R. Cingolani and R. Rinaldi, *Nature Nanotechnology*, 2006, **1**, 126.
38. S. M. Tabakman, L. Lau, J. T. Robinson, J. Price, S. P. Sherlock, H. Wang, B. Zhang, Z. Chen, S. Tangsombatvisit, J. A. Jarrell, P. J. Utz and H. Dai, *Nature Communications*, 2011, **2**, 466.
39. S. K. Jha, N. Mojarad, M. Agio, J. F. Löffler and Y. Ekinci, *Opt. Express*, 2015, **23**, 24719-24729.
40. D. J. Webb and C. M. Brown, *Methods in molecular biology (Clifton, N.J.)*, 2013, **931**, 29-59.
41. C. Stewart and J. Giannini, *Journal of Chemical Education*, 2016, **93**, 1310-1315.
42. Y. Hayashi, R. Matsuda, K. Ito, W. Nishimura, K. Imai and M. Maeda, *Analytical Sciences*, 2005, **21**, 167-169.
43. A. Shrivastava and V. Gupta, *Chronicles of Young Scientists*, 2011, **2**, 21-25.
44. J. Petruccelli and N. Davies, *Biometrika*, 1986, **73**, 687-694.

View Article Online
DOI: 10.1039/C8LC01344F

View Article Online
DOI: 10.1039/C8LC01344F

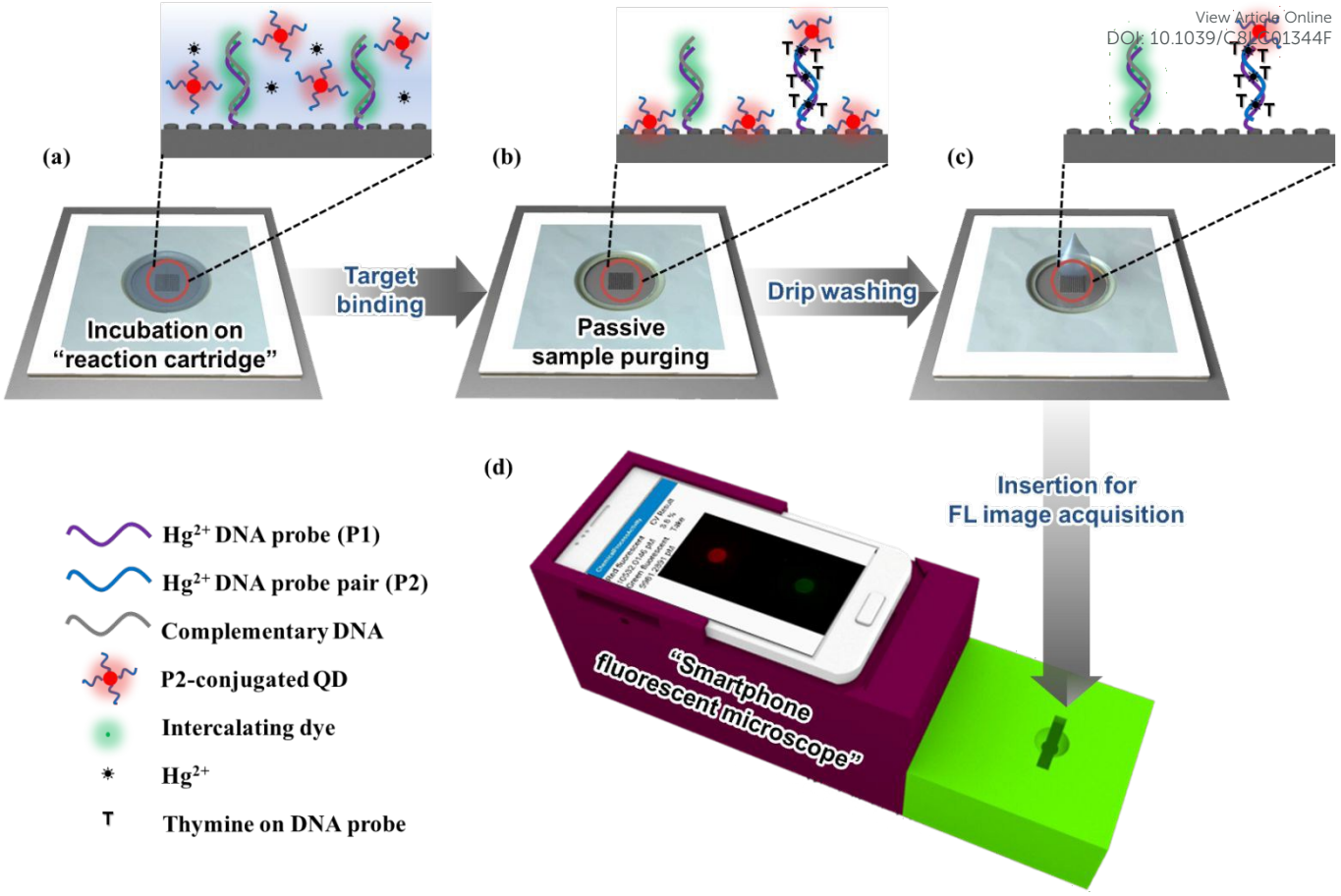

Fig. 1 Schematic illustration of the work. (a) P1 that is hybridized with cDNA and intercalated by SGI is printed on nano-structured substrate and starts to interact with Hg^{2+} and P2-conjugated QD during incubation in the center of the cartridge. (b) Passive sample purging occurs by the cartridge leaving reacted complex and unbound P2-conjugated QD. (c) Unbound reagent is washed by dripping washing buffer repeatedly. (d) After the process is completed, the cartridge is inserted to SFM for fluorescent image acquisition at red and green channel and then change of fluorescent intensity at each channel is analyzed, quantified and followed by display of detection result-out.

View Article Online
DOI: 10.1039/C8LC01344F

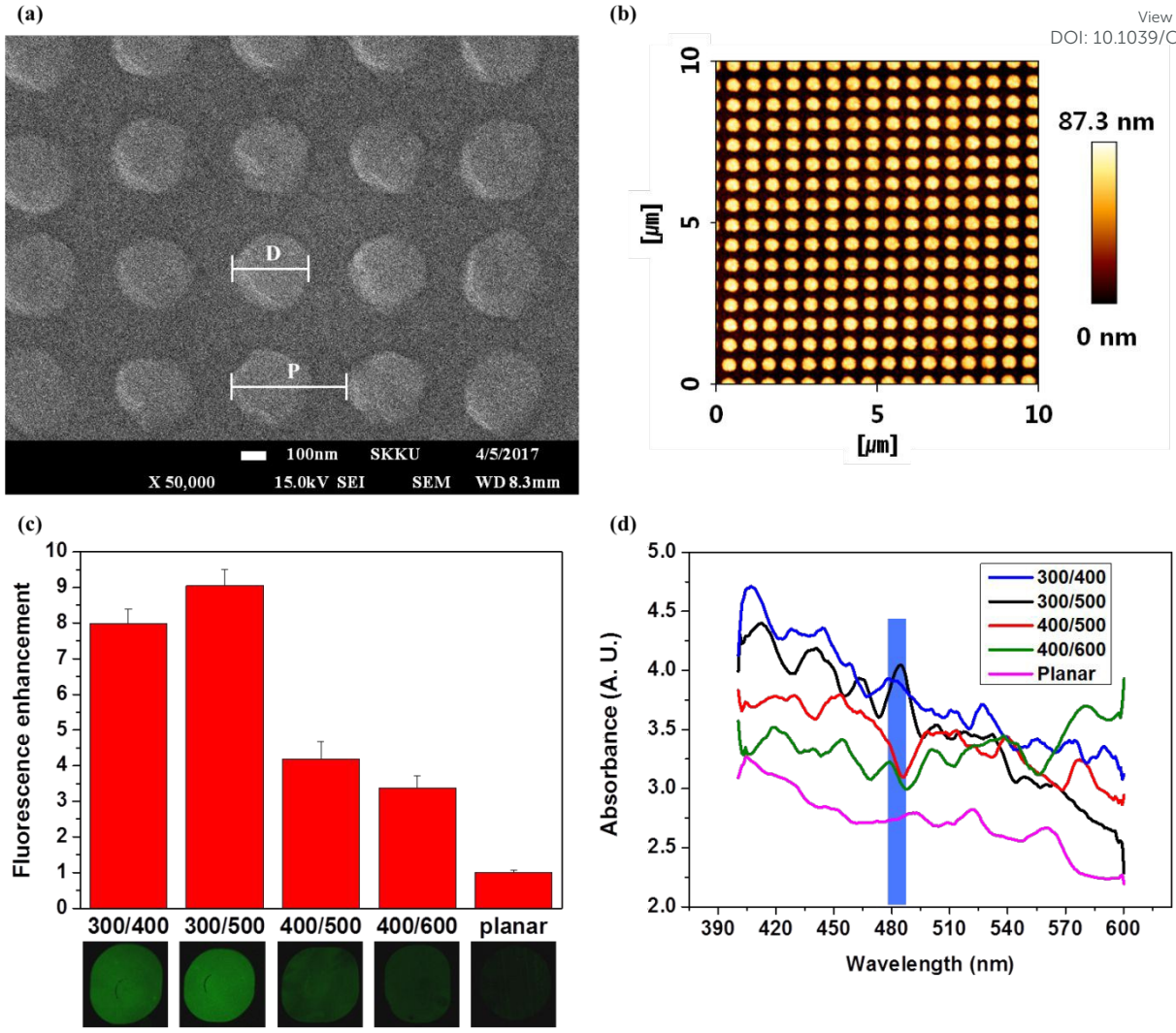

Fig. 2 Confirmation of nanopattern on polycarbonate substrate and its fluorescence enhancement response. (a) FESEM image of nanopillar array after deposition of 100 nm Ag and 30 nm Al_2O_3 thin films in turn. (scale bar, 100 nm). (b) AFM image of expanded area (100 μm²) on the substrate. (c) The fluorescence enhancement (F/F_0) response of nanopillar substrates with various D/P. Correspondingly, fluorescence images of microspot are presented below. (d) Comparison of the absorption spectra of substrates with different nanopatterns.

View Article Online
DOI: 10.1039/C8LC01344F

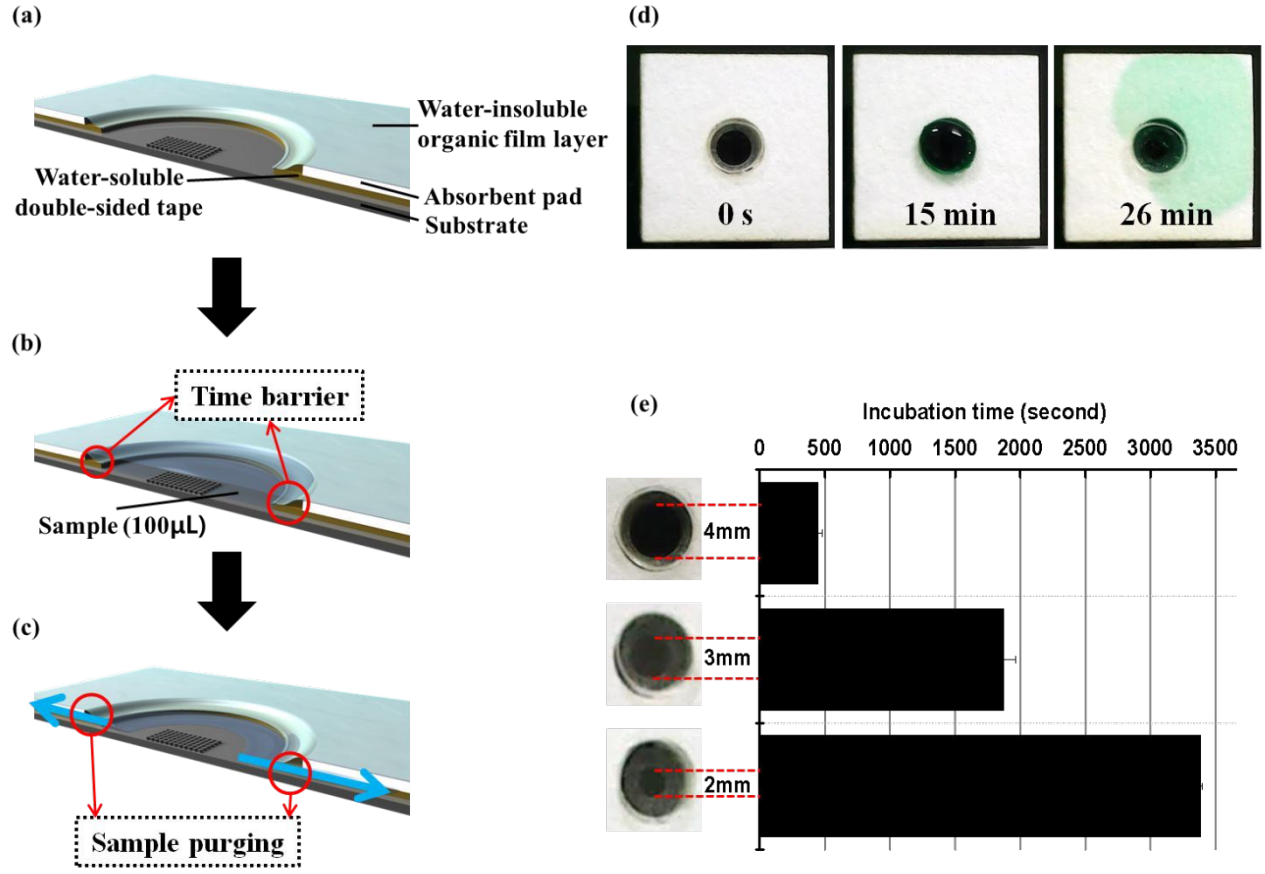

Fig. 3 Schematics for working principle of the novel biosensor cartridge and operational checkout. Illustration for structural and material sketch of the cartridge (a), time limit incubation (b), and passive sample purging (c). (d) Photograph of actual operation over time. (e) Controllability of incubation time by manipulating dimension of the center aperture.

View Article Online
DOI: 10.1039/C8LC01344F

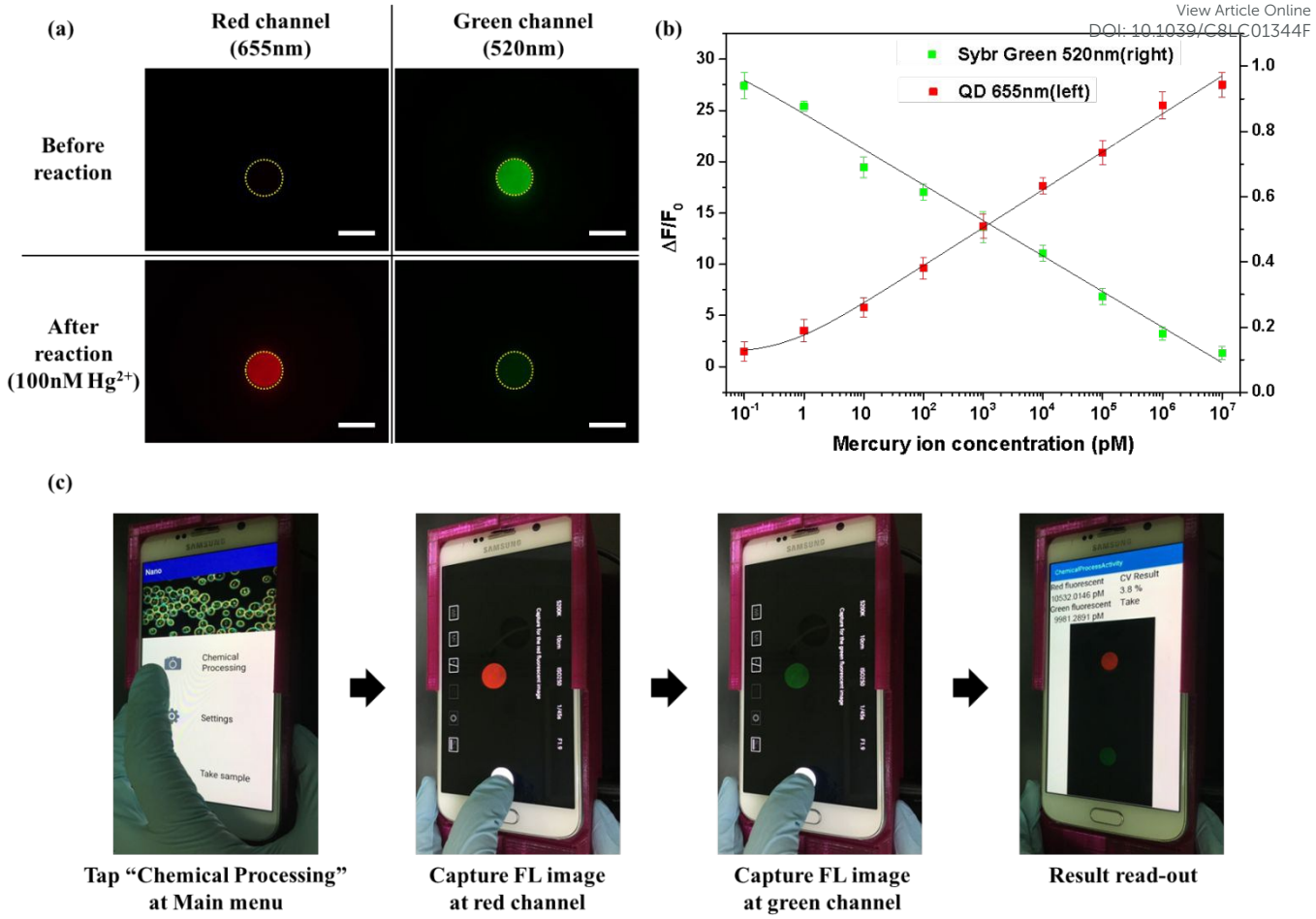

Fig. 4 Quantitative fluorescent imaging by SFM. (a) Example of fluorescent images acquired at red and green channel before and after reaction with 100 nM Hg^{2+} sample (scale bar, 300 μm). (b) Standard curves at red and green channel plotted with triplicate data and 3PL non-linear regression fitting. (c) Photographs of operation steps of the android app. for Hg^{2+} detection running on SFM. After tapping "Chemical Processing", user captures fluorescence image at red and green channel and then it displays detection result.

View Article Online
DOI: 10.1039/C8LC01344F

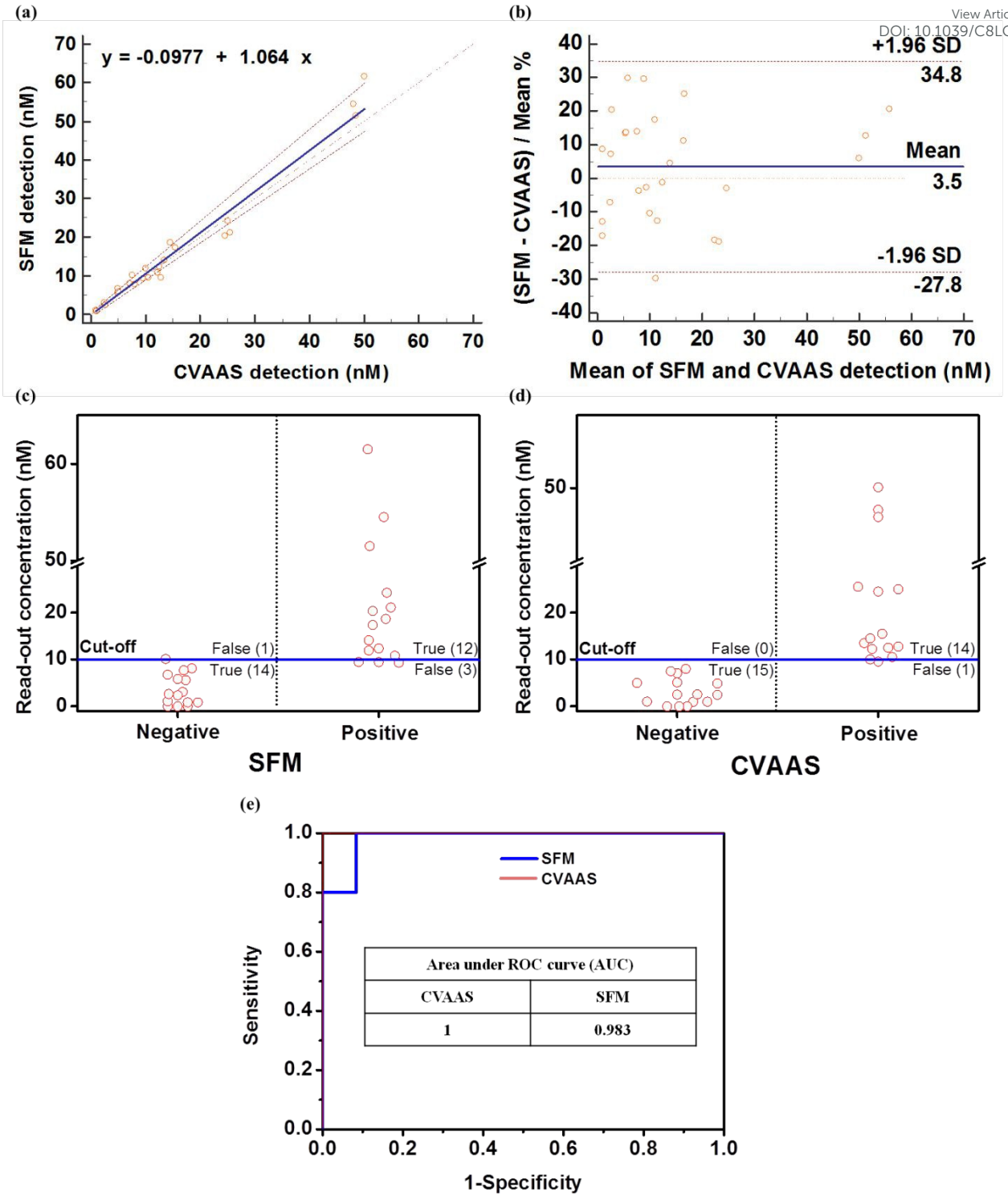

Fig. 5 Device evaluation of SFM compared to standard method, CVAAS. (a) Passing-Bablok analysis to compare Hg^{2+} concentration as measured by SFM and CVAAS. The center dashed line indicates the regression line, blue solid line represents the identity, and two dashed lines at the side indicate the confidence interval. (b) Bland-Altman analysis to compare the target detection results between SFM and CVAAS. The blue solid line represents the mean difference as percentage of the methods and two dashed lines indicate the 95% limit of agreements. The scattered plot shows how detection results are distributed in negative and positive groups below and above 10 nM for (c) SFM and (d) CVAAS. (e) Comparison of ROC curves for two methods.

View Article Online
DOI: 10.1039/C8LC01344F

Table of contents (TOC)

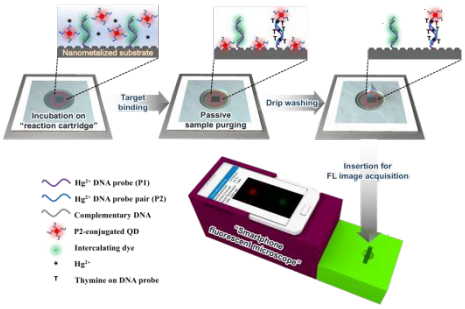

A biosensor cartridge adopting time-sequenced passive fluid handling was developed for Hg^{2+} detection with minimal user interventions and high accuracy.